Available online at www.sciencedirect.com
SCIENCE DIRECT®
Journal of Power Sources 139 (2005) 106–114
JOURNAL OF POWER SOURCES
www.elsevier.com/locate/jpowsour

Real-time water distribution in a polymer electrolyte fuel cell

Q. Dong, J. Kull, M.M. Mench*

Electrochemical Engine Center Fuel Cell Dynamics and Diagnostics Laboratory, Department of Mechanical and Nuclear Engineering, The Pennsylvania State University, University Park, PA 16802, USA

Received 15 June 2004; accepted 28 June 2004
Available online 13 September 2004

Abstract

Knowledge of the species distribution within a polymer electrolyte fuel cell (PEFC) is critical to fully characterize the local performance and accurately quantify the various modes of water transport. This paper describes the results of a newly developed real-time technique for in situ measurement of water vapor, nitrogen and oxygen distributions within the reactant flow channels of an operating PEFC using an Agilent real-time gas analyzer (RTGA). The RTGA was interfaced directly to the fuel cell at various locations along the single path serpentine anode and cathode flow channels of a specially designed fuel cell. Species distribution data are combined with measured high frequency resistance and current distribution. The periodic presence of liquid water droplets in the cathode at high current density and at locations near the cathode exit is also observed.

Keywords: Mass distribution; Water; Fuel cell; Flooding; Solid polymer electrolyte

1. Introduction

Many researchers have experimentally investigated the relationship between various operating conditions and performance of polymer electrolyte fuel cells (PEFCs) [1–14]. The reader is referred to refs. [15,16] for additional information on PEFC fundamentals. In addition to experimental research, first principle-based modeling of PEFCs has also been extensively developed in recent years [17–33]. At this stage, however, the experimental ability to validate the increasingly complex models is lagging behind the predictive capabilities. Real-time methods for experimental determination of species, temperature, current and other important parameters are needed to examine distributed and transient phenomena, and to provide precise benchmark data for detailed model validation. This work addresses the need for real-time species distribution data with a new experimental device that can be used to rapidly (1 Hz data acquisition frequency) conduct species profiling in an operating PEFC.

The species distribution within PEFC is critical for understanding the local performance of a PEFC because, at different locations, the same cell can be simultaneously suffering flooding, drying, and gas-phase transport limitations. This fact alone limits the quantitative usefulness of bulk approximations. Of particular interest is the water vapor distribution within the gas channels. The complex interrelated modes of water transport tend to dominate performance and stability, because electrolyte ionic conductivity increases with water content, but excess water will limit performance via flooding. Many researchers have conducted studies and developed models that describe the water transport through fuel cell components, including the electrolyte and porous gas diffusion layers [34–41]. In order to validate these models, the in situ mole fraction distribution of water vapor and other species within the gas channel is needed. A few authors have studied overall water balance in an operating fuel cell by collecting the fuel cell effluent, and condensing the gas-phase water vapor [42–45]. While insightful, these studies do not provide transient data on the water distribution throughout the cell, which could vary widely depending on operating conditions,

* Corresponding author. Tel.: +1 814 865 0060; fax: +1 814 863 4848.
E-mail address: mmench@psu.edu (M.M. Mench).

0378-7753/$ – see front matter © 2004 Elsevier B.V. All rights reserved.
doi:10.1016/j.jpowsour.2004.06.068

current distribution and local non-isotropic transport parameters.

In a recent work, Mench et al. [46] demonstrated the ability to accurately measure the in situ water vapor mole fraction distribution in an operating PEFC with an Agilent 3000 MicroGC Gas Chromatograph, without the need for condensation of the water vapor. While this technique provides molar percent level accuracy of the water vapor content across the flow channels, it still requires on the order of 5 min per data point, and has limited accuracy for low levels of some important species such as CO. Thus, the utility of this technique is still essentially limited to analyzing steady state species distribution. In order to enable the study of species transport dynamics in the fuel cell, it is necessary to decrease the time between consecutive data points by another order of magnitude, while increasing accuracy.

In this paper, the ability to measure various species including water vapor, nitrogen and oxygen in near real time (∼1 s per data point) is demonstrated with an Agilent real-time gas analyzer system. The 300-fold decrease in data collection time compared to the MicroGC method makes it possible to continuously monitor species mole fraction changes at selected locations along the anode or cathode flowpath, and also provides detailed understanding and perspective of the time scales of the various intercoupled multi-phase dynamic transport phenomena.

Since water generation is directly proportional to current density, it is also desirable to couple water and current distribution measurements to provide detailed information on non-uniform transport and generation effects. This can be accomplished with a segmented cell approach, developed and described in refs. [47,48]. Along with current and species distribution, high frequency resistance (HFR) distribution can be used to reveal the local ionic conductivity (and thus hydration state) of the electrolyte. This is accomplished in this study with a multi-channel 3 kHz ac impedance analyzer that scans the same areas where current density is measured through the segmented cell technique.

2. Experimental

In order to accurately measure the hydrogen, oxygen, nitrogen, and water species present in the fuel cell, a G3163A real-time gas analyzer (RTGA) was utilized (Agilent Technologies Inc.). A continuous flow of sample gas mixture (<3% of total gas mixture in the fuel cell) was diverted from the fuel cell to the RTGA. Using the RTGA eliminates the need for gas species separation. The sample line temperature from fuel cell to the RTGA was monitored and kept well above 100 °C (typically 150 °C), to prevent condensation of water vapor in the sample line. Since low-pressure gas flow can hold a greater mole fraction of water than higher-pressure gas flow, there is no condensation resulting from the pressure drop from the fuel cell location to the RTGA inlet. Depending on the pressure of the fuel cell, the average delivery time for species from the fuel cell to the RTGA was determined to be around 0.3 s, based on calculations of sample line interior volume and known flow rate.

A 50 cm^2 active area fuel cell was utilized in this study. The fuel cell has a single channel, serpentine design and is segmented to allow simultaneous current density distribution measurements, as described in refs. [47,48]. Further specific details and geometry of the instrumented fuel cell are given in ref. [49]. Fig. 1 is a schematic diagram detailing the relevant dimensions of the fuel cell. The dimension of the flow channel was chosen to be 2.2 mm in width, 3.2 mm in depth, and has an average pass length of approximately 71 mm.

The membrane electrode assembly (MEA) used for testing was provided by W.L. Gore and Associates, with carbon paper GDL on the anode and cathode, and an electrolyte thickness of 18 μm. Other standard operating conditions for the data presented are given in Table 1 for reference. Ultra-high purity (>99.999%) hydrogen and breathing grade air were supplied from compressed gas-cylinders. The multi-channel potentiostat used in this work was manufactured by Arbin Instruments (College Station, Texas) and also provides humidity, temperature, pressure, and flow rate control.

For species distribution measurements, eight species extraction ports are located along the anode and cathode serpentine paths of the specialized fuel cell. They are positioned within the 1st, 4th, 7th, 10th, 13th, 16th, 19th and 22nd reactant channel passes at 4.3, 17.4, 30.4, 43.5, 56.5, 69.6, 82.6 and 95.7% of the fractional distance along the single serpentine path from the channel inlet, respectively. To reduce water droplet blockage and false readings, the extraction takes place along the back wall of the polycarbonate retaining plate, at the farthest distance from the MEA.

3. Results and discussion

3.1. RTGA calibration and measurement

Calibration was conducted before every set of experiments, and is accomplished with ultra-high purity gasses and an adiabatic saturation device for water quantification. The adiabatic saturator is operated at extremely low flow rate and precisely known temperature and pressure, to ensure a known humidity of the calibration gas mixture. For water vapor calibration, a single point calibration is made at a humidifier exit temperature of around 50 °C, and the measured ion response signal is correlated to the water vapor mole fraction determined through thermodynamic calculation. Then, the temperature of the adiabatic saturator is increased, and the calibration is checked against the theoretical value to ensure accuracy.

A calibration curve taken for fully humidified airflow is shown in Fig. 2. The calibration curves shown are based on a bottled air mixture at 2.4 atm (20.6 psig) humidification

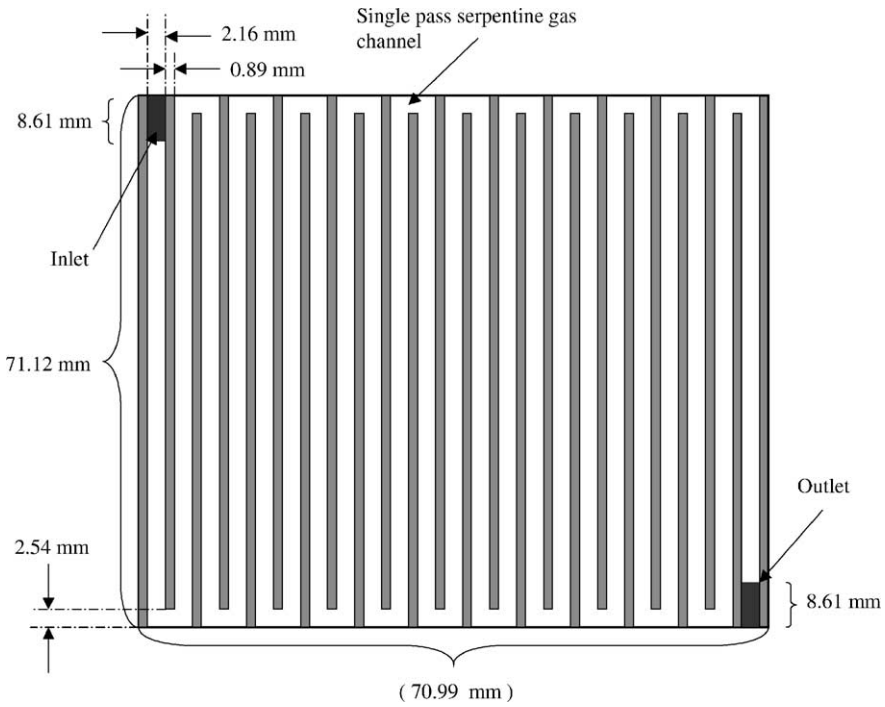

Fig. 1. Schematic diagram of the 50 cm^2 instrumented test cell with relevant dimensions shown.

pressure. The theoretical data are calculated based on thermodynamics of saturated mixtures. The average measured mole fraction is within ±0.5% mole fraction of the theoretical value, up to very high values of water mole fraction at 90 °C. This compares to a scatter of ±5.0% mole fraction observed with the GC in ref. [34].

Fig. 3 shows a plot of the measured ion count (which correlated to the mole fraction via calibration) versus time as the adiabatic saturator set-point temperature is increased in discreet increments. At the bottom of the chart, minute amounts of carbon dioxide and argon are observed. This is a result of the impurities present in the industrial air cylinder used. Typical values for Ar and CO_2 impurities in the grade of commercial cylinders used range from 0 to 1800 and 0 to 2 ppm, respectively. The fact that a measurable signal is generated for these minor species demonstrates the precision of the RTGA device. Following the water vapor ion count with time, oscillation can be observed, with increasing amplitude as the humidification set-point temperature is increased. It is interesting to note that this variation in the signal corresponds to measured adiabatic saturator set point temperature oscillation, not measurement uncertainty. This variation is also observed to varying degrees in humidification systems used in fuel cells. Additional calibrated data shows that this oscillation can amount to ±1% mole fraction of water vapor in the flow channels, depending on operating condition

Table 1
Baseline operating conditions

Parameter	Value	Units
Electrolyte	GORE PRIMEA® (18 μm)	NA
Gas diffusion layer	ELAT® (E-TEK of De Nora North America) anode and cathode	NA
Catalyst loading (carbon supported)	0.5	mg cm^{-2}
Cell temperature	80	°C
Anode inlet temperature	80	°C
Cathode inlet temperature	80	°C
Cathode flow rate	2.0	A cm^{-2} equivalent
Anode flow rate	1.5	A cm^{-2} equivalent
Cathode pressure	30	psig
Anode pressure	30	psig
Cathode inlet humidity	50% at 80 °C	NA
Anode inlet humidity	100% at 80 °C	NA
Anode gas	Ultra high purity H_2 (>99.999%)	NA
Cathode gas	Breathing air (79% N_2, 21% O_2)	NA

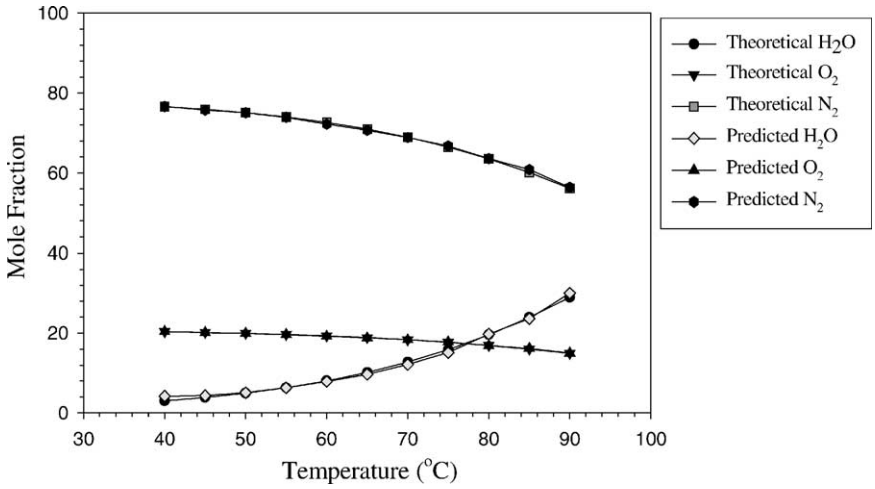

Fig. 2. Comparison between measured and theoretical water vapor, oxygen and nitrogen concentrations. Measured with baseline calibration value at 50 °C. The adiabatic saturator was at 2.4 atm (20.6 psig) pressure.

and location. This indicates that the inlet vapor mole fraction may not always be suitably approximated as constant, depending on the humidification apparatus, and with a function best characterized experimentally.

3.2. Benchmark data

Figs. 4–6 show the measured water, nitrogen and oxygen mole fraction at locations of 4.3, 56 and 83% along the single channel cathode flowpath, respectively. The species distributions in these figures are plotted as a function of time, for three fuel cell voltages of 0.8, 0.65 and 0.5 V. The measured current distribution associated with these measurements is shown in Fig. 7. The fuel cell was operated under the conditions listed in Table 1. This series of tests were designed to illustrate: (1) the effect of a dynamic change in current density on the water, nitrogen and oxygen mole fractions; (2) the increase of water saturation and concomitant formation of water droplets along the cathode flowpath.

It can be seen from Fig. 4 (at 4.3% along the cathode flowpath—essentially the entrance), that local conditions are dominated by cathode inlet flow, and here current density has little effect on the gas-channel level liquid saturation. Also, the increase in fuel cell current density (which accompanies the controlled decrease in cell voltage from 0.7 to 0.65 and 0.5 V), has little effect on channel mole fraction due to the high local stoichiometry at the inlet location. That is, only a small fraction of the total reactant flow has been consumed by this entrance location.

Fig. 5 presents data taken at 56% along the cathode flowpath—essentially the middle of the flowpath. At this location, the current density has a definite effect on the fractions of water, nitrogen and oxygen. The approximate time scale

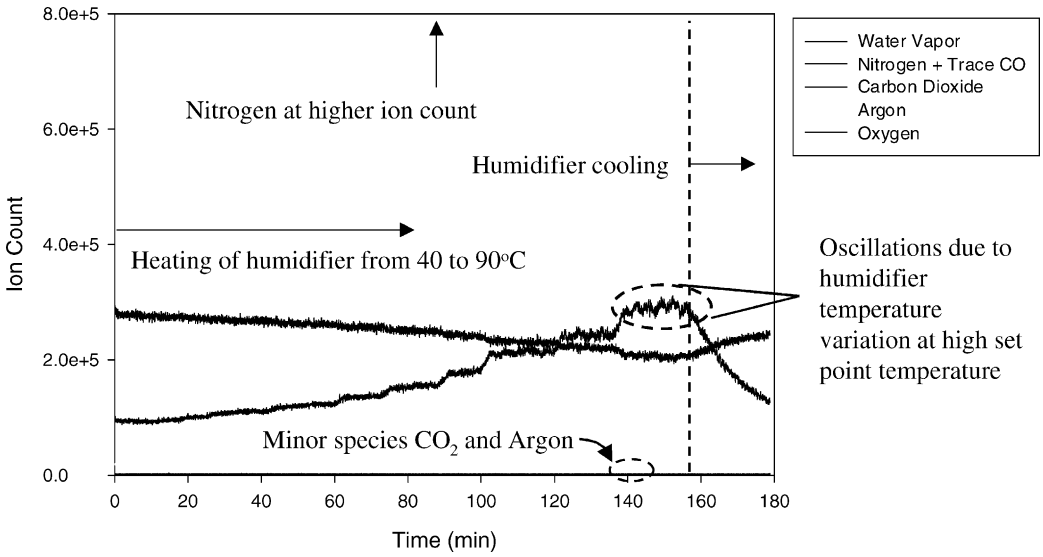

Fig. 3. Plot of ion count measured by RTGA vs. time as the adiabatic saturator set-point temperature is increased in discreet increments from 40 to 90 °C.

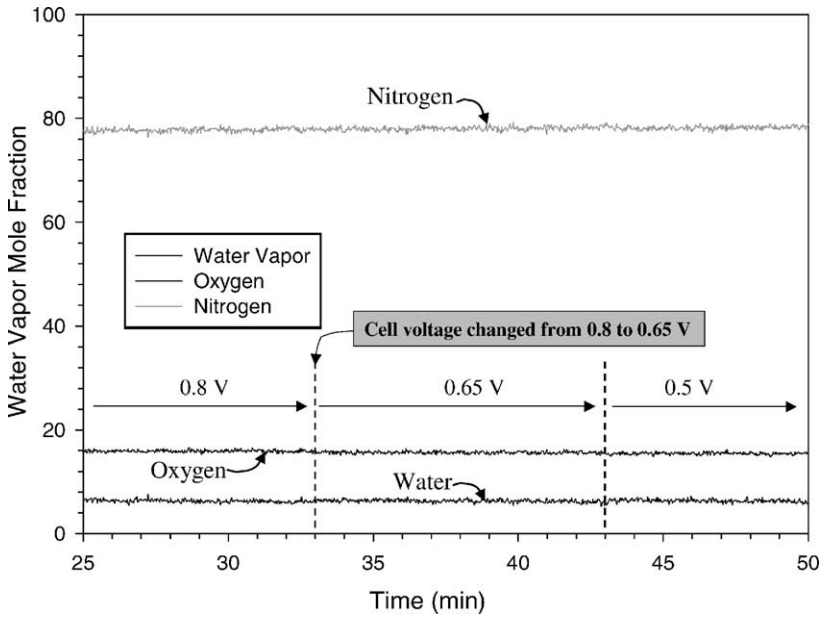

Fig. 4. Water vapor distribution at a distance of $x/L = 0.043$ along cathode serpentine flowpath. Changes in cell voltage are marked by the vertical dashed lines from 0.8 to 0.65 V and 0.65 to 0.5 V.

of gas-phase channel flow adjustment (∼1 min) can be seen from this figure by comparing the voltage adjustment time to the gas-phase adjustment time. Subsequent work will quantify this parameter in more detail, since it was not rigorously recorded in this preliminary study. It is interesting to note the presence of spikes in the species mole fraction. This is a result of sporadic water droplet entrainment into the RTGA sample line, and is evidence of the emergence of liquid water droplets on the gas diffusion layer (GDL) and in the cathode flow channel. At 0.8 V (low bulk current density of about 0.2 A cm^{-2}), there are no droplets measured over 10 min time at this location. When the cell voltage is lowered to 0.65 V (higher bulk current density of ∼0.6 A cm^{-2}), liquid droplets emerge at this location midway along the cathode flowpath, with a frequency of about one spike every 10 min. When the cell voltage is lowered to 0.50 V (highest bulk current density of ∼0.65 A cm^{-2}), liquid droplets are recorded more frequently, corresponding to the higher generation rate of water. At this voltage, the frequency of liquid water droplets is about once every 4–5 min.

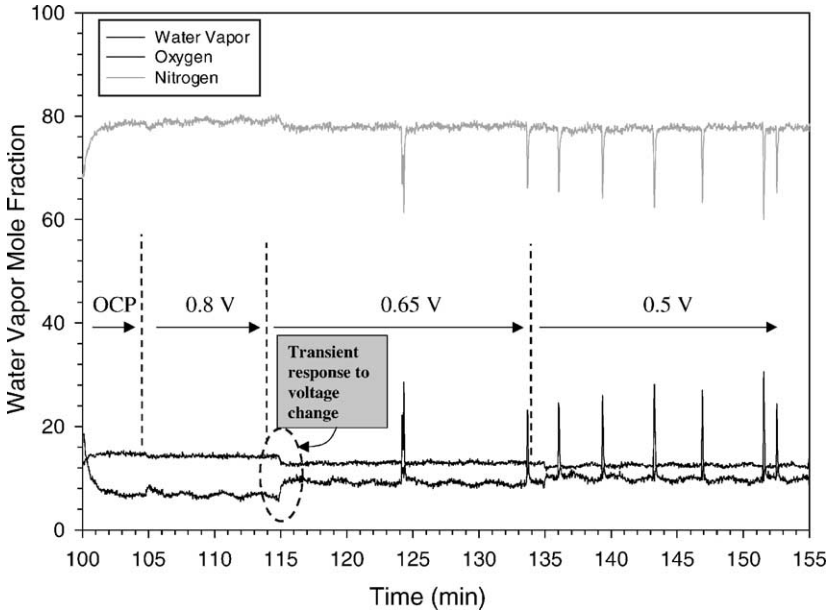

Fig. 5. Water vapor distribution at a distance of $x/L = 0.565$ along cathode serpentine flowpath. The portion of the plot circled with a dashed line highlights the transient response to the change in voltage. Spikes in mole fraction data are indicative of the presence of liquid droplets in the flow channel.

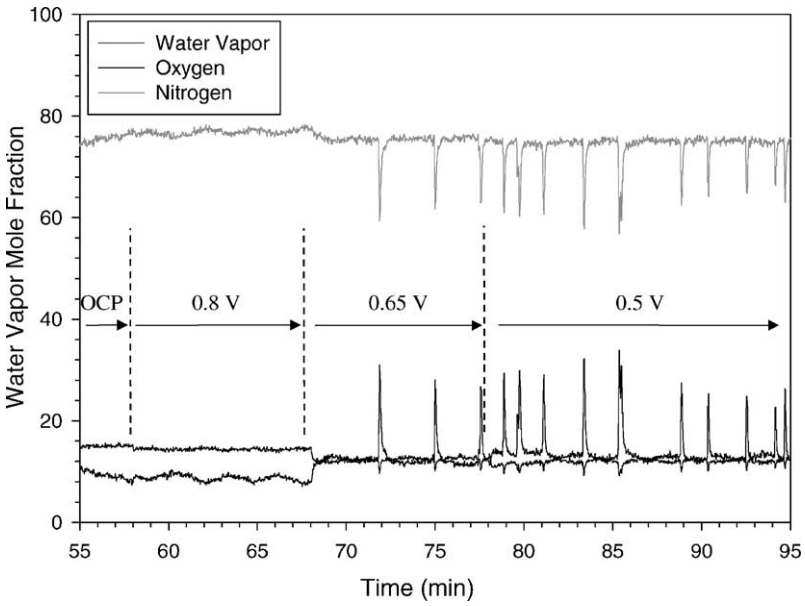

Fig. 6. Water vapor distribution at a distance of x/L = 0.826 along cathode serpentine flowpath. More liquid droplet peaks are evident at this downstream location near the cathode channel exit.

Fig. 6 presents data taken at 82.6% along the cathode flowpath—near the outlet of the fuel cell. At this location, the current density has a very strong effect on the fractions of water, nitrogen and oxygen, as expected. There is clearly a strong dependence of oxygen and nitrogen mole fraction on current density, as the longer path length increases the integrated water uptake and species consumption. Compared to Fig. 5, the same trend from 0.8 to 0.5 V is observed in terms of liquid droplets. At 0.8 V, there are no droplets measured over 15 min time. When the cell voltage is lowered to 0.65 V, liquid droplets emerge with a frequency of about once every 3 min, compared to one every 10 min for the mid-channel location shown in Fig. 5. When the cell voltage is lowered to 0.50 V, liquid droplets are observed at a frequency of about once every 1–2 min. These data are especially valuable for two-phase modeling that predicts droplet growth and transport.

Figs. 7 and 8 show the distributed current density and high frequency resistance (HFR measured at 3 kHz) for the same test conditions listed in Table 1, respectfully. Recall

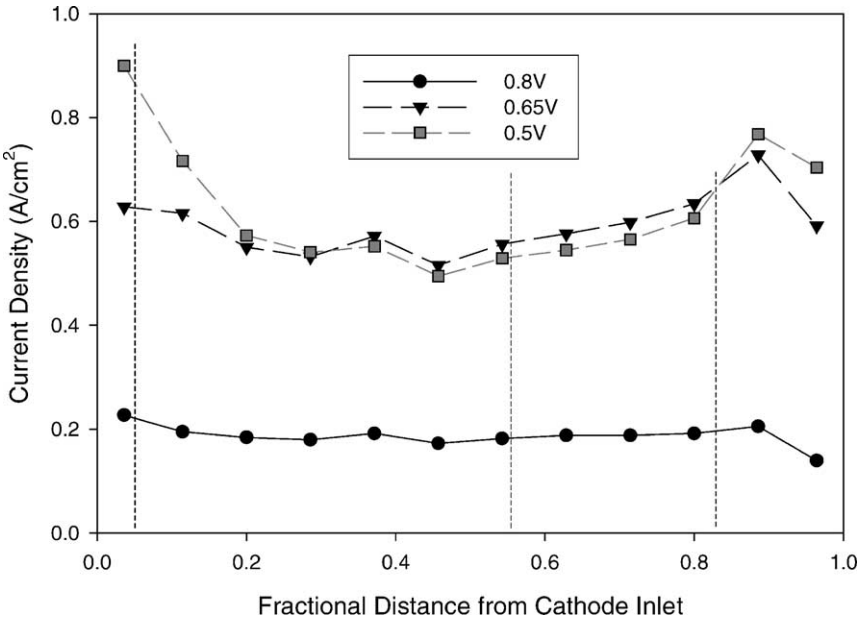

Fig. 7. Plot of current density vs. the fractional distance from the cathode inlet at different voltages. The vertical dashed lines represent the different sampling port locations shown in Figs. 4–6.

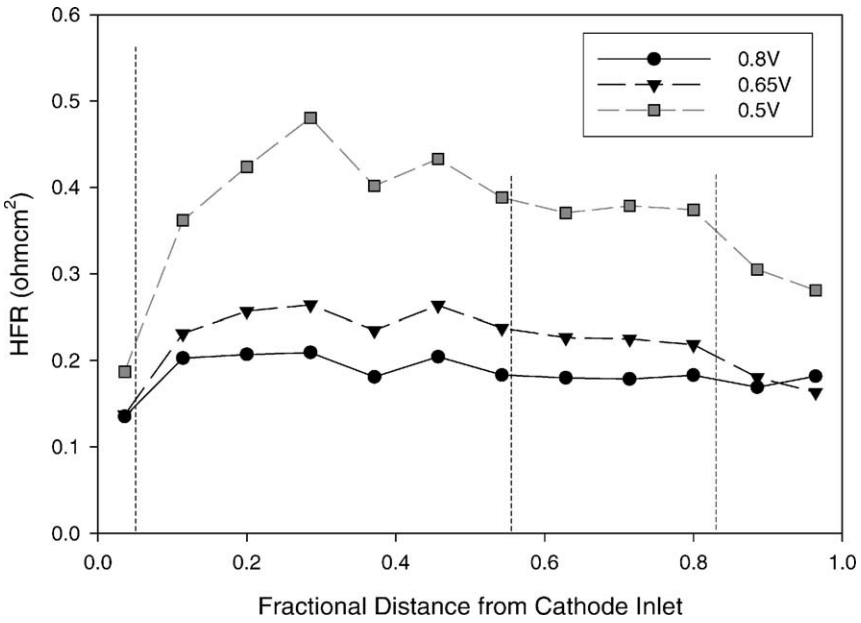

Fig. 8. Plot of high frequency resistance distribution (3 kHz) vs. fractional distance from the cathode inlet at different voltages. The vertical dashed lines represent the different sampling port locations shown in Figs. 4–6.

that the inlet humidity of the cathode is 50% at 80 °C, and the anode inlet is 100% RH at 80 °C. The current density for the case of 0.8 and 0.65 V is generally homogeneously distributed. The HFR shows a similar trend. For the case of 0.5 V, the bulk current density is higher than the 0.65 V case, but in the middle of the cell, it is slightly lower. The high initial current density at the inlet of the fuel cell for the 0.5 V case apparently results in anode dryout, for increased current density and diffusion to the dry cathode, and associated high HFR. The combination of HFR, current density and species distributions at the same test conditions represent a set of detailed benchmark data for model validation.

Fig. 9 shows the steady state water uptake for three cell voltages as functions of fractional distance from the cathode inlet for the same test conditions. Each point shown here represents the average of at least 5-min continuous data. For a cell voltage, due to water generation, electro-osmotic drag and water diffusion from the anode to the dry cathode, cathode water mole fraction increased along the flowpath. Since both water generation and electro-osmotic drag are directly related to current density, it can be seen from the figure that cell voltage has significant effect on cathode water uptake, as indicated by the liquid droplet emerging frequency variation shown in Figs. 5 and 6. Lower cell voltage resulted in higher

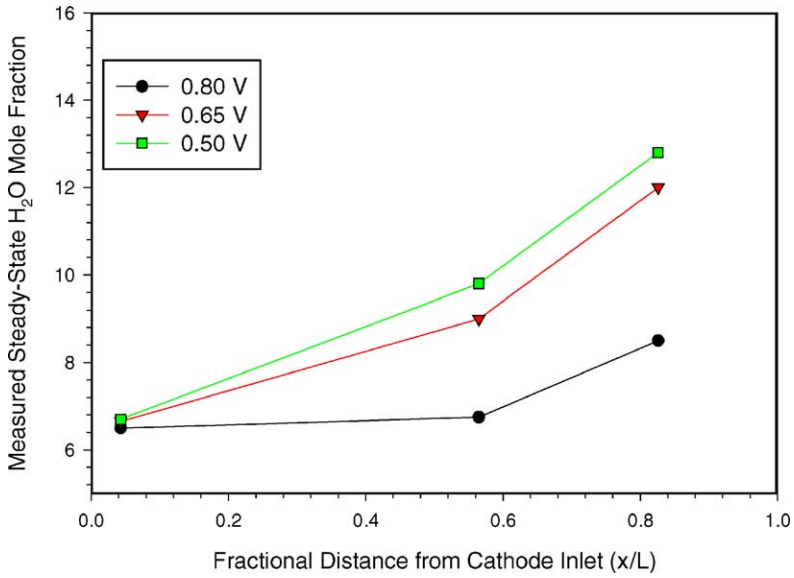

Fig. 9. Plot of the steady state water vapor uptake in the cathode flow channel vs. the fractional distance along cathode flowpath for three fuel cell voltages.

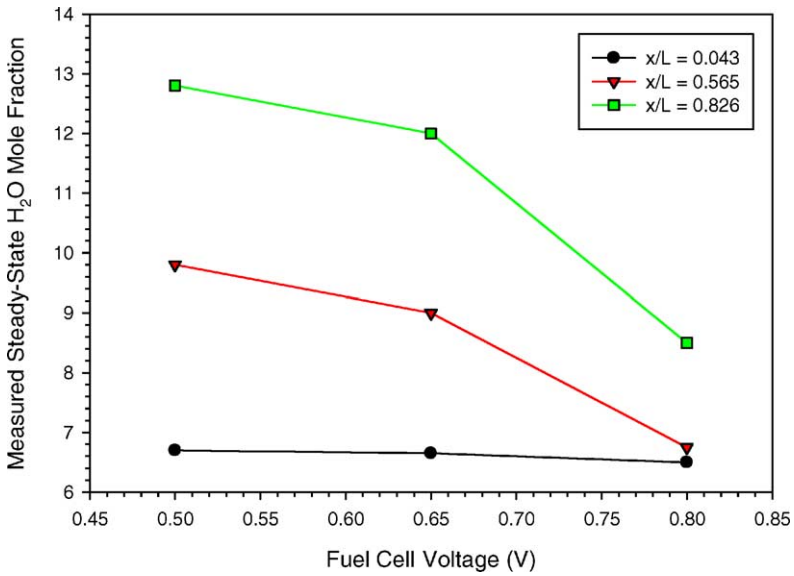

Fig. 10. Plot of the steady state water vapor uptake in the cathode flow channel vs. fuel cell voltage for three different fractional distances through the cathode flowpath.

water content due to the higher respective current density. For the cases of 0.65 and 0.5 V, the water mole fractions are close because of their close current densities,

Fig. 10 shows the steady state water mole fraction for three sampling locations as functions of cell voltage. Each point in the figure still represents the average of at least 5-min continuous data shown in Figs. 4–6. It can be seen that the water mole fraction at a sampling location is directly related to the current density and the upstream membrane area of the location. For the position at 4.3% along the cathode flowpath, cell voltage did not show obvious effect on cathode water mole fraction due to the small membrane area in front of the location.

4. Conclusions

An Agilent real-time gas analyzer (RTGA) has been calibrated and interfaced to a PEFC to enable rapid and precise measurement of species distribution in real time. This technique can be used to directly profile water and other species in the anode and cathode of an operating fuel cell and also directly capture the transient gas-phase channel level adjustment to changes in other operating conditions, such as current density. This new technique was used with existing experimental diagnostics for distributed current and high frequency resistance measurement to generate a set of detailed benchmark data. The presence of liquid water droplets on the GDL surface was observed through water vapor signal peaks. As expected, more cathode-side water droplets are present as current is increased or the location is more toward the cathode exit. Considering the high accuracy of measuring various species, this new diagnostic technique is presently being used by the author's laboratory to study many important phenomena in great detail, especially water transport dynamics.

Acknowledgements

Funding for the experimental work and the RTGA equipment was provided by Agilent Technologies Inc. Special thanks to Donna Mazur, Vince Giarrocco, Ron Henner and Brooke Miller for their assistance. Funding for Mr. Jon Kull was provided by the Penn State Schreyer's Honor College Program. The authors also wish to thank Mr. Dan Shields for his help in setting up the laboratory equipment. The membrane electrode assemblies used in this research were provided by W.L. Gore and Associates.

References

[1] D.M. Bernardi, J. Electrochem. Soc. 137 (1990) 3344.
[2] A. Parthasarathy, S. Srinivasan, A.J. Appleby, C. Martin, J. Electrochem. Soc. 139 (1992) 2530.
[3] A. Parthasarathy, S. Srinivasan, A.J. Appleby, C. Martin, J. Electrochem. Soc. 139 (1992) 2856.
[4] Y.W. Rho, O.A. Velev, S. Srinivasan, Y.T. Kho, J. Electrochem. Soc. 141 (1994) 3838.
[5] J.C. Amphlett, R.M. Baumert, R.F. Mann, B.A. Peppley, P.R. Roberge, T.J. Harris, J. Electrochem. Soc. 142 (1995) 9.
[6] R. Mosdale, S. Srinivasan, Electrochim. Acta 40 (1995) 413.
[7] H.-F. Oetjen, V.M. Schmidt, U. Stimming, F. Trila, J. Electrochem. Soc. 143 (1996) 3838.
[8] T.E. Springer, T.A. Zawodzinski, M.S. Wilson, S. Gottesfeld, J. Electrochem. Soc. 143 (1996) 587.
[9] F.N. Büchi, S. Srinivasan, J. Electrochem. Soc. 144 (1997) 2767.
[10] E.A. Ticianelli, C.R. Derouin, S. Srinivasan, J. Electroanal. Chem. 251 (1988) 275.

[11] F.A. Uribe, S. Gottesfeld, T.A. Zawodzinski, J. Electrochem. Soc. 149 (2002) 293.
[12] E. Antolini, R.R. Passos, E.A. Ticianelli, J. Appl. Electrochem. 32 (2002) 383.
[13] M. Fournier, J. Hamelin, K. Agbossou, T.K. Bose, Fuel Cells 2 (2002) 117.
[14] L. Wang, A. Husar, T. Zhou, H. Liu, Int. J. Hydrogen Energy 28 (2003) 1263.
[15] J. Larminie, A. Dicks, Fuel Cell Systems Explained, John Wiley and Sons Ltd., New York, 2002.
[16] S. Gottesfeld, in: C. Tobias (Ed.), Advances in Electrochemical Science and Engineering, vol. 5, John Wiley and Sons, New York, 1997.
[17] T.E. Springer, T.A. Zawodinski, S. Gottesfeld, J. Electrochem. Soc. 138 (1991) 2334.
[18] D.M. Bernardi, M.W. Verbrugge, AIChE J. 37 (1991) 1151.
[19] D.M. Bernardi, M.W. Verbrugge, J. Electrochem. Soc. 139 (1992) 2477.
[20] T.E. Springer, M.S. Wilson, S. Gottesfeld, J. Electrochem. Soc. 140 (1993) 3513.
[21] T.F. Fuller, J. Newman, J. Electrochem. Soc. 140 (1993).
[22] T.V. Nguyen, R.E. White, J. Electrochem. Soc. 140 (1993) 2178.
[23] C.Y. Wang, W.B. Gu, J. Electrochem. Soc. 145 (1998) 3407.
[24] V. Gurau, H. Liu, S. Kakac, AIChE J. 44 (1998) 2410.
[25] J.S. Yi, T.V. Nguyen, J. Electrochem. Soc. 146 (1999) 38.
[26] S. Um, C.Y. Wang, K.S. Chen, J. Electrochem. Soc. 147 (2000) 4485.
[27] C.Y. Wang, S. Um, H. Meng, U. Pasaogullari, Y. Wang, 2002 Fuel Cell Seminar Abstracts (2002) 33.
[28] Q. Guo, V.A. Sethuraman, R.E. White, J. Electrochem. Soc. 151 (A 983) (2004) 3981.
[29] A.A. Kulikovsky, J. Divisek, A.A. Komyshev, J. Electrochem. Soc. 146 (1999) 3981.
[30] S. Um, C.Y. Wang, J. Power Sources 125 (2004) 40.
[31] P. Berg, K. Promislow, J. Pierre, J. Stumper, B. Wetton, J. Electrochem. Soc. 151 (2004) 341.
[32] L. Pisani, G. Murgia, M. Valentini, B. D'Aguanno, J. Electrochem. Soc. 149 (2002) 898.
[33] A.Z. Weber, J. Newman, J. Electrochem. Soc. 151 (2004) 311.
[34] D.M. Bernardi, J. Electrochem. Soc. 137 (1990) 3344.
[35] T.E. Springer, T.A. Zawodzinski, S. Gottesfeld, J. Electrochem. Soc. 138 (1991) 2334.
[36] D.M. Bernardi, M.W. Verbrugge, J. Electrochem. Soc. 139 (1992) 2477.
[37] T.F. Fuller, J. Newman, J. Electrochem. Soc. 140 (1993) 1218.
[38] M. Eikerling, Y.I. Kharkats, A.A. Kornyshev, Y.M. Volfkovich, J. Electrochem. Soc. 145 (1999) 2684.
[39] J.S. Yi, T.V. Nguyen, J. Electrochem. Soc. 146 (1999) 38.
[40] I.-M. Hsing, P. Futerko, Chem. Eng. Sci. 55 (2000) 4209.
[41] Z.H. Wang, C.Y. Wang, K.S. Chen, J. Power Sources 94 (2001) 40.
[42] X. Ren, S. Gottesfeld, J. Electrochem. Soc. 148 (2001) 87.
[43] G.J. Janssen, J. Electrochem. Soc. 148 (2001) 1313.
[44] G.J. Janssen, M.L. Overvelde, J. Power Sources 101 (2001) 117.
[45] W.-k. Lee, J.W. Van Zee, S. Shimpalee, S. Dutta, Proceedings of ASME Heat Transfer Division, vol. 1, 1999, p. 339.
[46] M.M. Mench, Q.L. Dong, C.Y. Wang, J. Power Sources 124 (2003) 90.
[47] M.M. Mench, C.Y. Wang, J. Electrochem. Soc. 150 (2003) 79.
[48] M.M. Mench, C.Y. Wang, M. Ishikawa, J. Electrochem. Soc. 150 (9) (2003) 1052.
[49] O.H. Finckh, M.S. thesis, The Pennsylvania State University, 2002.